# Role of Net Surface Heat Flux in Seasonal Variations of Sea Surface Temperature in the Tropical Atlantic Ocean

LISAN YU, XIANGZE JIN, AND ROBERT A. WELLER

*Department of Physical Oceanography, Woods Hole Oceanographic Institution, Woods Hole, Massachusetts*

(Manuscript received 4 November 2005, in final form 11 April 2006)

ABSTRACT

The present study used a new net surface heat flux ($Q_{net}$) product obtained from the Objective Analyzed Air–Sea Fluxes (OAFlux) project and the International Satellite Cloud Climatology Project (ISCCP) to examine two specific issues—one is to which degree $Q_{net}$ controls seasonal variations of sea surface temperature (SST) in the tropical Atlantic Ocean (20°S–20°N, east of 60°W), and the other is whether the physical relation can serve as a measure to evaluate the physical representation of a heat flux product. To better address the two issues, the study included the analysis of three additional heat flux products: the Southampton Oceanographic Centre (SOC) heat flux analysis based on ship reports, and the model fluxes from the National Centers for Environmental Prediction–National Center for Atmospheric Research (NCEP–NCAR) reanalysis and the 40-yr European Centre for Medium-Range Weather Forecasts (ECMWF) Re-Analysis (ERA-40). The study also uses the monthly subsurface temperature fields from the World Ocean Atlas to help analyze the seasonal changes of the mixed layer depth ($h_{MLD}$).

The study showed that the tropical Atlantic sector could be divided into two regimes based on the influence level of $Q_{net}$. SST variability poleward of 5°S and 10°N is dominated by the annual cycle of $Q_{net}$. In these regions the warming (cooling) of the sea surface is highly correlated with the increased (decreased) $Q_{net}$ confined in a relatively shallow (deep) $h_{MLD}$. The seasonal evolution of SST variability is well predicted by simply relating the local $Q_{net}$ with a variable $h_{MLD}$. On the other hand, the influence of $Q_{net}$ diminishes in the deep Tropics within 5°S and 10°N and ocean dynamic processes play a dominant role. The dynamics-induced changes in SST are most evident along the two belts, one of which is located on the equator and the other off the equator at about 3°N in the west, which tilts to about 10°N near the northwestern African coast.

The study also showed that if the degree of consistency between the correlation relationships of $Q_{net}$, $h_{MLD}$, and SST variability serves as a measure of the quality of the $Q_{net}$ product, then the $Q_{net}$ from OAFlux + ISCCP and ERA-40 are most physically representative, followed by SOC. The NCEP–NCAR $Q_{net}$ is least representative. It should be noted that the $Q_{net}$ from OAFlux + ISCCP and ERA-40 have a quite different annual mean pattern. OAFlux + ISCCP agrees with SOC in that the tropical Atlantic sector gains heat from the atmosphere on the annual mean basis, where the ERA-40 and the NCEP–NCAR model reanalyses indicate that positive $Q_{net}$ occurs only in the narrow equatorial band and in the eastern portion of the tropical basin. Nevertheless, seasonal variances of the $Q_{net}$ from OAFlux + ISCCP and ERA-40 are very similar once the respective mean is removed, which explains why the two agree with each other in accounting for the seasonal variability of SST.

In summary, the study suggests that an accurate estimation of surface heat flux is crucially important for understanding and predicting SST fluctuations in the tropical Atlantic Ocean. It also suggests that future emphasis on improving the surface heat flux estimation should be placed more on reducing the mean bias.

*Corresponding author address:* Lisan Yu, Department of Physical Oceanography, Woods Hole Oceanographic Institution, MS#21, Woods Hole, MA 02543.
E-mail: lyu@whoi.edu

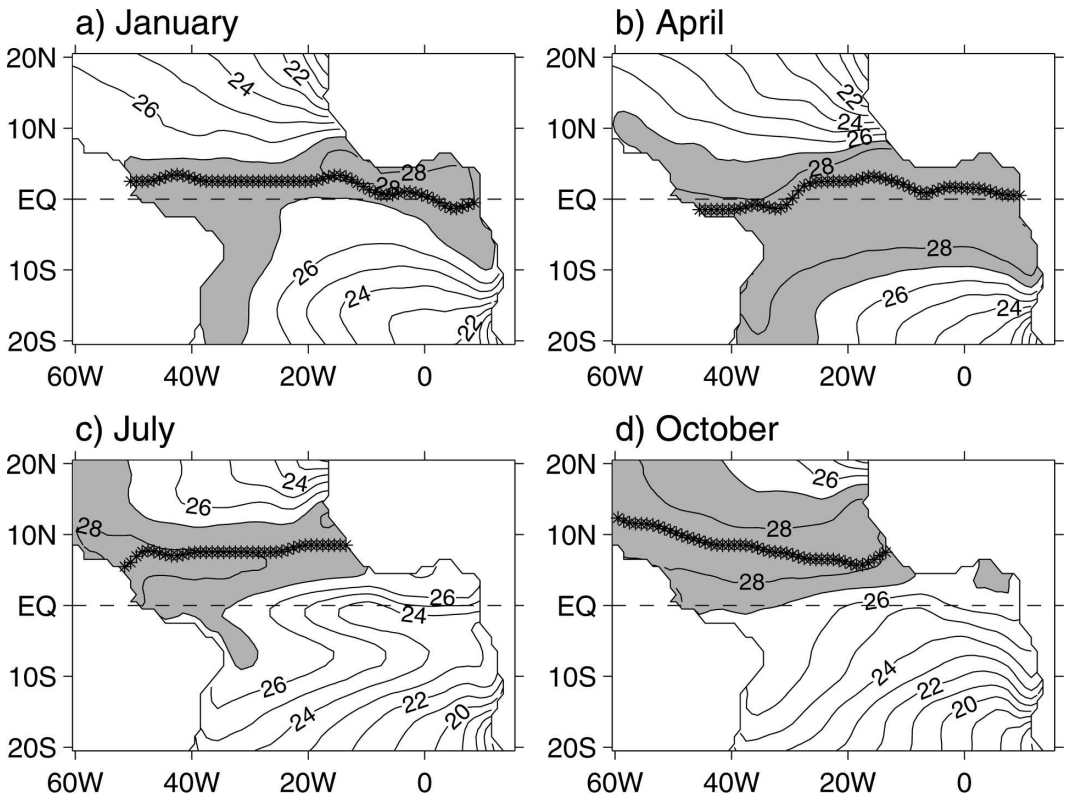


FIG. 1. Distribution of SST (contours in °C) and its relation to the ITCZ location (thick black line) in (a) January, (b) April, (c) July, and (d) October. Contour interval for SST is 1°C and SST higher than 27°C is shaded. The superimposed thick black contour denotes the mean position of the ITCZ for the respective month, which is defined as the position of the precipitation maximum in the monthly climatology of the Xie and Arkin merged precipitation analysis (1997). SST data are taken from the OAFlux product.

## 1. Introduction

The seasonal location of the intertropical convergence zone (ITCZ) controls much of the seasonal variations of the tropical Atlantic Ocean (Hastenrath and Lamb 1978; Merle 1980; Merle and Arnault 1985; Houghton 1983, 1991; Garzoli and Katz 1983; Molinari et al. 1985; Hastenrath and Merle 1987; Katz 1987; Richardson and Reverdin 1987; Weingartner and Weisberg 1991a,b; Philander et al. 1996; Carton and Zhou 1997; Wang and Enfield 2001; Foltz et al. 2003; Xie and Carton 2004; Joyce et al. 2004). Take the sea surface temperatures (SSTs) as an example (Fig. 1). As the ITCZ migrates north and south annually, from about 10°N in the boreal fall to about 3°N in the boreal spring, the pool of high SSTs (>27°C) moves accordingly so that the warm water pool is always located underneath the ITCZ. It is known that the ITCZ is a region of deep atmospheric convection, heavy precipitation, low solar heating, and weak mean wind speed. How the atmosphere interacts with the ocean to create the seasonal sea surface warming underlying the ITCZ has long been a focal subject of many studies.

Merle (1980) first noted from the archived Nansen datasets that the seasonal variations of the equatorial Atlantic SST were not similar to changes in the subsurface heat content. Several other observational analyses (Merle 1980; Garzoli and Katz 1983; Hastenrath and Merle 1987; Reverdin et al. 1997) further evidenced that the warming of the sea surface is not always associated with large subsurface heat content related to the thermocline deepening. Houghton (1991), based on expendable bathythermograph (XBT) data along four shipping lanes that cross the basin from 30°N to 20°S from 1980 to 1987, showed that a warm SST is correlated with a shallow thermocline everywhere except in the eastern equatorial region. His finding suggested that for most of the tropical Atlantic Ocean the dynamic state beneath the surface mixed layer has only a limited influence on the annual cycle of SST. His finding also suggested that a shallow thermocline does not necessarily facilitate cooling of the mixed layer; instead, it can foster a warming of the sea surface.

The fact that the SST increase is associated with a shallow thermocline indicates that the major contribu-

tor to the surface mixed layer heat budget is not the vertical flux of heat through the thermocline but the net surface heat flux through the air–sea interface (i.e., the combination of net shortwave radiation, latent and sensible heat loss, and net longwave emission). This supports the idea originated from Niiler and Kraus (1977) that surface heating has a role in reducing near-surface mixing, thus reducing heat loss at the base of the mixed layer and modulating the mixed layer temperature (equivalently, the temperature of sea surface). Such a role of surface heat flux in driving seasonal variations of SST has been demonstrated by several ocean model studies (Seager et al. 1988; Giese and Cayan 1993; Köberle and Philander 1994) for the tropical oceans that are off the equator and away from the coast. In these regions much of the net surface heat flux is stored locally in the upper layer, and the seasonal change of SST can be modeled by simply relating the local heat flux with a variable mixed layer depth (Moisan and Niiler 1998).

On the other hand, the tropical atmosphere and ocean are a coupled entity, and feedback interaction between the ocean and the atmosphere should be at the heart of the SST seasonality (Hastenrath 1984). Indeed, the annual formation of the equatorial cold tongue is the result of the positive atmosphere–ocean interaction. The mechanism, which is established by Mitchell and Wallace (1992) from observational evidence, states that the onset of the Northern Hemisphere summer monsoons and its interactions with the underlying upwelling of cold water are instrumental in reestablishing and maintaining the seasonal occurrence of the cold SST in the eastern equatorial region. The mechanism has been supported by many model studies (e.g., Chang and Philander 1994; Chang 1996; Wang 1994; Carton and Zhou 1997; Nigam and Chao 1996), as well as observational evidence. For instance, Weingartner and Weisberg (1991a,b) conducted 1-yr field observations at a central equatorial location (28°W). They showed that the sharp reduction in SST in the boreal spring is induced by upwelling associated with seasonally enhanced easterlies. At this location, although surface heat flux is not a dominant forcing for cooling the sea surface, they showed that the warming of the sea surface in boreal winter is in response to the increase of surface heat flux in a shallow mixed layer. Apparently, surface heat flux contributes to the warming part of the annual cycle of SST even in the deep Tropics where dynamic air–sea feedback interaction plays a central role.

Given that the high correlation between warm SST and shallow thermocline occurs when the vertical heat flux through the thermocline is weak, the dominant influence of surface heat flux on seasonal variations of SST can be modeled by relating the two variables with a variable mixed layer depth through the following expression:

$$\mathrm{dSST} = \frac{dt}{\rho c_p}\frac{Q_{\mathrm{net}}}{h_{\mathrm{MLD}}}, \tag{1}$$

where dSST represents the SST change over a time interval $dt$ (taken as 1 month) when there is a net surface heat flux $Q_{\mathrm{net}}$ distributed throughout the mixed layer of thickness $h_{\mathrm{MLD}}$; $\rho$ is the seawater density and $c_p$ is the heat capacity of seawater. The model has been applied by several studies to explain the role of local heating in the observed SST fluctuations on annual, seasonal, and interannual time scales. These applications include McPhaden (1982) for the central equatorial Indian Ocean, Leetmaa (1983) for the eastern tropical Pacific, Houghton (1991) for four volunteer observing ship (VOS) routes crossing the tropical Atlantic, Moisan and Niiler (1998) for the North Pacific, and Frankignoul and Hasselmann (1977) for the study of SST feedbacks on seasonal time scales.

Theoretically, dSST can be predicted by using (1) once $Q_{\mathrm{net}}$ is known. In reality, $Q_{\mathrm{net}}$ from existing sources, such as flux climatologies derived from the Comprehensive Ocean–Atmosphere Data Set (COADS; Woodruff et al. 1993), flux fields produced from numerical weather prediction (NWP) models, and flux products generated from satellite measurements, all contain uncertainties. Because of the concern that the large inconsistencies between these datasets could lead to a misrepresentation of the mixed layer heat balance, most studies created their own fluxes either from in situ surface meteorological measurements at limited locations (e.g., Merle 1980; Molinari et al. 1985; Houghton 1991; Weingartner and Weisberg 1991a,b; Foltz et al. 2003) or by using the coupled models (e.g., Chang and Philander 1994; Xie 1994; Wang 1994; Carton and Zhou 1997; DeWitt and Schneider 1999).

Efforts have been made in recent years to develop improved surface heat flux estimates. A new set of surface heat flux fields has been derived from the Objectively Analyzed Air–Sea Fluxes (OAFlux) project by the Woods Hole Oceanographic Institution (WHOI) through combining satellite observations with in situ measurements and outputs of surface meteorological fields from NWP reanalysis models (Yu et al. 2004a). Synthesizing data from different sources cancels out the errors in input data and can result in an optimal estimate that has the minimum error variance. Validation analyses (Yu et al. 2004b) have shown that the synthe-

sized OAFlux products represent an improvement over the NWP flux fields and the COADS-based flux climatologies in both mean and variability. At present, daily latent and sensible heat flux estimates on a 1° grid have been produced for the years from 1980 to present. To compute net heat flux for this study, surface shortwave and longwave radiation from the International Satellite Cloud Climatology Project (ISCCP) (i.e., the ISCCP-FD dataset) (Zhang et al. 2004) are obtained. The ISCCP-FD radiation was calculated from a complete radiative transfer model from the Goddard Institute for Space Studies (GISS) GCM using ISCCP observations (Zhang et al. 2004) and is available every 3 h over the whole globe on a 2.5° grid from July 1983 to June 2001. A linear interpolation in space was applied to project the ISCCP-FD data onto the OAFlux 1° grid. The two datasets are part of the most recent global heat flux products; together they enable the computation of a net surface heat flux climatology (OAFlux + ISCCP dataset) for the overlapping period of 1984–2000.

The present study takes advantage of these new development efforts and addresses two specific objectives. First, much of the understanding of the seasonal response of the tropical Atlantic SST to surface heat flux is gained from in situ measurements at limited locations and regions. The study will investigate whether the SST and surface heat flux relationship derived from the new flux dataset is consistent with existing knowledge. Second, considerable differences exist between OAFlux + ISCCP and NWP reanalysis model fluxes and the COADS-based flux climatology. The study will investigate whether the relation (1) can be served as a physical constraint to characterize the physical representativeness of heat flux field products. Therefore, the study includes the analysis of three additional heat flux products: one is the COADS-based climatology from Southampton Oceanographic Center (SOC; Josey et al. 1998, 1999), and the other two are the NWP model fluxes from National Centers for Environmental Prediction–National Center for Atmospheric Research (NCEP–NCAR) reanalysis (Kalnay et al. 1996) and the 40-yr European Centre for Medium-Range Weather Forecasts (ECMWF) Re-Analysis (ERA-40; Uppala et al. 1999).

The paper is organized as follows. Section 2 gives a brief description of the data information required by the relation (1). The seasonal variations of $Q_{\text{net}}$, $h_{\text{MLD}}$, and dSST are presented in section 3. The correlation relationship between $Q_{\text{net}}$ and dSST is examined in section 4, and the role of $h_{\text{MLD}}$ in modulating the relationship is also discussed. The seasonal prediction of SST based on relation (1) is attempted in section 6. Summary and discussions are given in section 7.

## 2. Data

Relation (1) requires the following three sets of data information: net surface heat flux $Q_{\text{net}}$, dSST, and the mixed layer depth $h_{\text{MLD}}$. As discussed in the previous section, four sets of $Q_{\text{net}}$ are to be examined. This includes the newly developed OAFlux + ISCCP (Yu et al. 2004a,b; Zhang et al. 2004), the COADS-based SOC climatology (Josey et al. 1999), and the two atmospheric reanalysis fluxes from NCEP–NCAR (Kalnay et al. 1996) and ERA-40 (Uppala et al. 1999), respectively. The SOC climatology was based on the 18-yr COADS data record from 1980 to 1997. The other datasets are time dependent with data records covering at least the past 25 yr, except for ISCCP, which is available only from July 1983 to June 2001. To take into account the ISCCP availability, the climatology of $Q_{\text{net}}$ from OAFlux + ISCCP, NCEP–NCAR, and ERA-40 was constructed for the period from 1984 to 2000.

The four sets of the mean $Q_{\text{net}}$ climatology in the tropical Atlantic Ocean are shown in Fig. 2. In this study, positive (negative) $Q_{\text{net}}$ denotes an oceanic heat gain (loss). Clearly, the four mean $Q_{\text{net}}$ patterns are quite different in terms of how much heat the tropical Atlantic Ocean receives on the annual mean basis. OAFlux + ISCCP and SOC both show that the annual mean $Q_{\text{net}}$ is positive over the entire sector from 20°S to 20°N, while the two NWP models indicate that the positive $Q_{\text{net}}$ occurs in a smaller region, that is, the equatorial belt and the eastern portion of the basin. Despite the large difference in the mean, all of the products are consistent in projecting that $Q_{\text{net}}$ is at the maximum in the equatorial region and $Q_{\text{net}}$ decreases toward high north and south latitudes.

Here dSST was defined as the differences between the mean of the last 5 days and the first 5 days of the month. The computation can be easily done for OAFlux + ISCCP, NCEP–NCAR, and ERA-40, because all three sources have SST with high temporal resolution. The 6-hourly NWP SST fields were interpolated from the Reynolds et al. (2002) weekly objective interpolated SST (OISST) analysis, while the daily OAFlux SSTs were generated from the synthesis of daily averages of satellite SST from the Advanced Very High Resolution Radiometer (AVHRR) and the NWP SST fields. The three SST fields have a long-term mean that is in good agreement with that of the OISST analysis (Yu et al. 2004b). On the other hand, SOC has only monthly mean SST fields. To calculate dSST, daily SOC SSTs were obtained by linearly interpolating the monthly means.

The mixed layer depth fields were derived from climatological monthly mean profiles of potential tem-

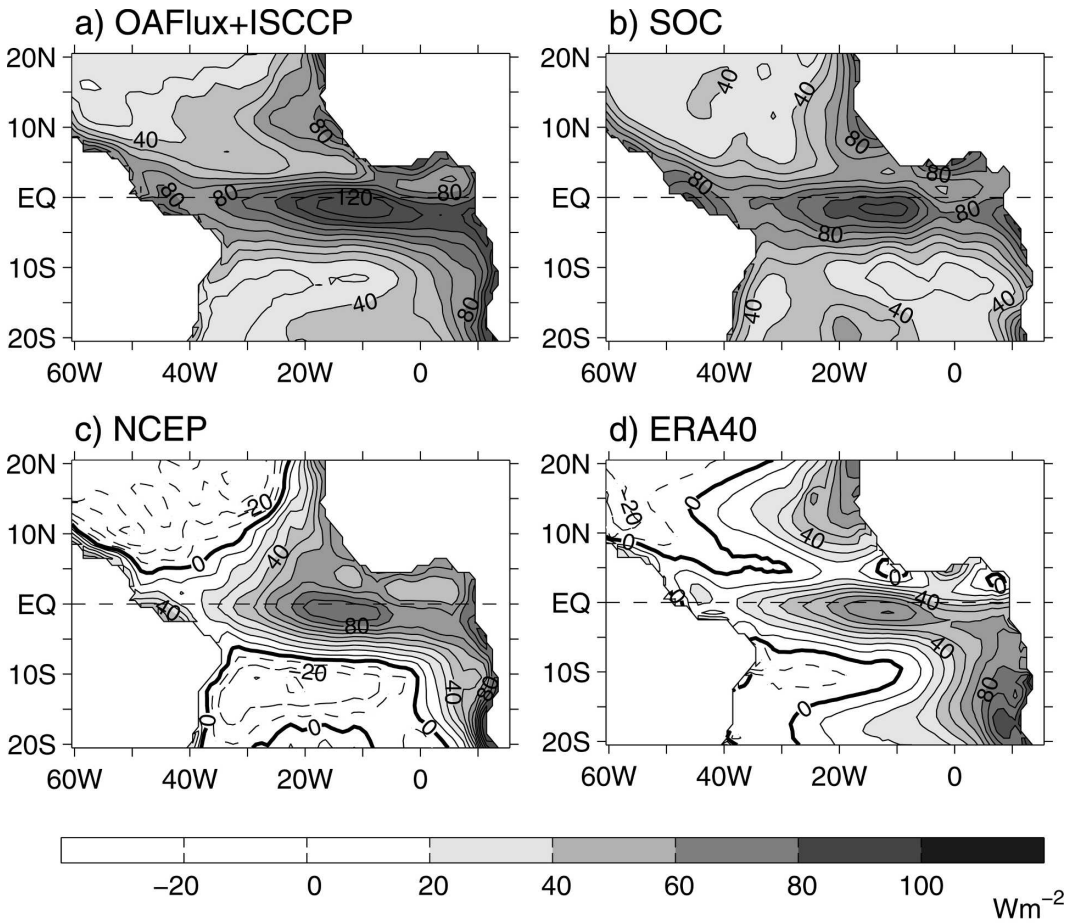


FIG. 2. Annual mean of $Q_{net}$ produced by (a) OAFlux + ISCCP, (b) SOC, (c) NCEP–NCAR, and (d) ERA-40. Contour interval is 10 W m$^{-2}$, with negative contours dashed, positive contours solid, and zero contours bold solid.

perature of the *World Ocean Atlas 1998* (WOA; Levitus et al. 1994). A linear interpolation was applied to infer the mixed layer depth as the depth at which temperature is 0.5°C below the SST (Foltz et al. 2003). This definition of the mixed layer depth enables the vertically averaged mixed layer temperature very close to SST but neglects vertical mixing at the base of the mixed layer.

In summary, the analysis of relation (1) will be based on four sets of $Q_{net}$ climatology and will use dSST from the same four sources. Because all of the four heat flux components are dependent of SST $Q_{net}$ and SST are internally coupled. Using $Q_{net}$ and dSST from the same data source will eliminate issues related to data inconsistency. The mixed layer depth $h_{MLD}$ is the only dataset that is independent of any of the four flux sources.

## 3. Seasonal variations of $Q_{net}$, dSST, and $h_{MLD}$

Seasonal variations of the three variables are examined by using the standard deviation (STD), that is, the square root of variance. Figure 3 plots the STD of the four sets of $Q_{net}$ with respect to their own annual mean. Interestingly, compared to the four annual mean fields (Fig. 2), the four STD fields have a much better agreement in both the pattern and amplitude. All products show that the amplitude of the $Q_{net}$ seasonal variations is minimum at the order of 10–20 W m$^{-2}$ along the narrow equatorial band between 5°S and 5°N and the off the South African coast, and that the amplitude increases poleward away from the equator. Although details of the pattern vary with the product and no two patterns are exactly alike, all, except NCEP–NCAR, seem to agree that the equatorial minimum amplitude belt is zonally aligned.

The STD of dSST based on the OAFlux dataset is shown in Fig. 4a. Unlike $Q_{net}$, the dSST from the four data sources (i.e., OAFlux, SOC, NCEP–NCAR, and ERA-40) are very similar in both mean and variability and hence, only the STD of the OAFlux dSST is shown. To delineate the relation to the ITCZ, Fig. 4a is superimposed with the annual mean position of the ITCZ,

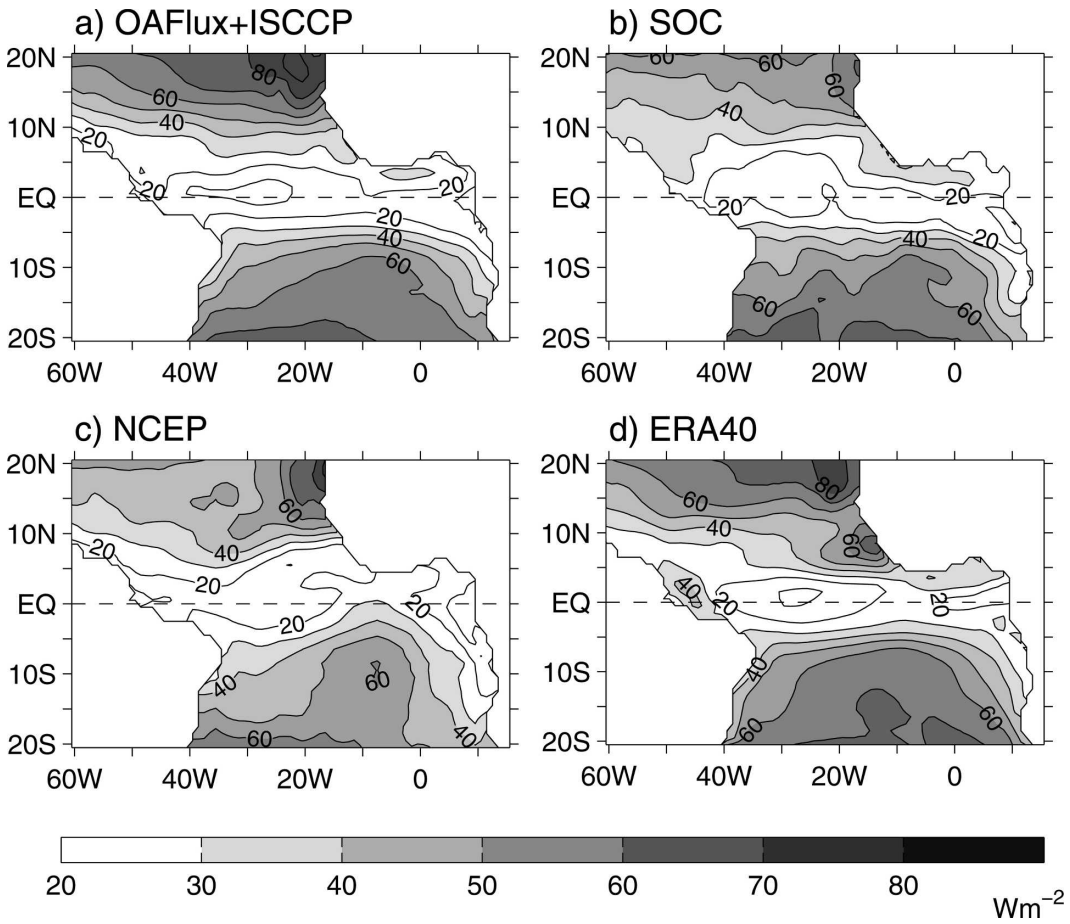


FIG. 3. STD of $Q_{net}$ computed from (a) OAFlux + ISCCP, (b) SOC, (c) NCEP–NCAR, and (d) ERA-40. Contour interval is 10 W m$^{-2}$.

which is defined as the position of the precipitation maximum in the monthly climatology of Xie and Arkin's (1997) merged precipitation analysis. It can be seen that the mean ITCZ location is situated at approximately 5°N and acts as a thermal equator, that is, the mean ITCZ location is the center location of maximum annual mean SSTs (Fig. 1) and minimal dSST (and SST) variances (Figs. 4a–b). Large dSST (and SST) variances are located on the two sides of the thermal equator, with one maximum off the northwest African coast and the other off the southwest African coast. Both dSST and SST have a similar STD pattern (Fig. 4b), except that the amplitude of the seasonal dSST variations is smaller; dSST represents the rate of the change in SST. The STD measures the departure of the monthly mean with respect to the annual mean. For those locations where SST monthly anomalies are small, one also anticipates that the rate of the change in SST (i.e., dSST) is small. It is therefore expected that, though the STD of the two variables have different amplitudes, the patterns should be similar.

In contrast to the STD of dSST, which has large variances in the east, the STD of $h_{MLD}$ (Fig. 5a) shows small variances in the east. This contrasting feature was first noted by Merle (1980) and further analyzed by Hastenrath and Merle (1987), and altogether they found that high variability of SST in the eastern part of the basin is related to a shallow mixed layer (see Fig. 5b) and a thin and intense thermocline associated with oceanic upwelling. The two shallowest $h_{MLD}$ regions are located on the two sides of the mean ITCZ position, between which there exists a belt of deeper $h_{MLD}$ in broad concordance with the mean ITCZ position. Hastenrath and Merle (1987) showed that this belt of relatively deeper $h_{MLD}$ is related to the seasonal development of the North Equatorial Countercurrent (NECC).

## 4. Relationship between dSST and $Q_{net}$

### *a. Seasonal covariability between $Q_{net}$ and dSST*

Figure 6 displays the month-to-month evolution of dSST with the monthly $Q_{net}$ from OAFlux + ISCCP

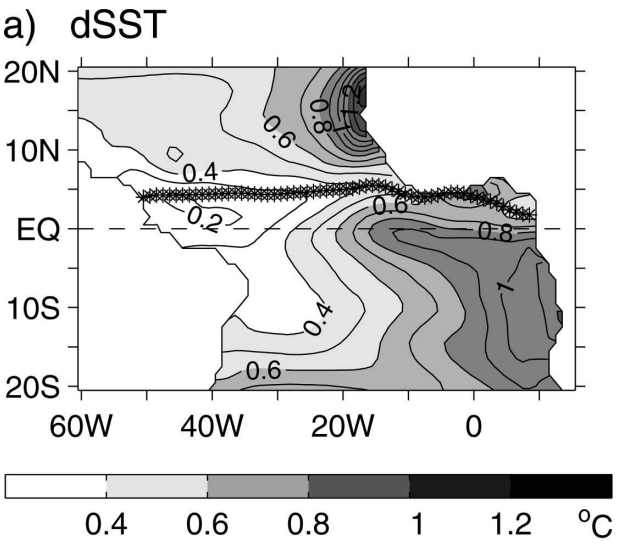


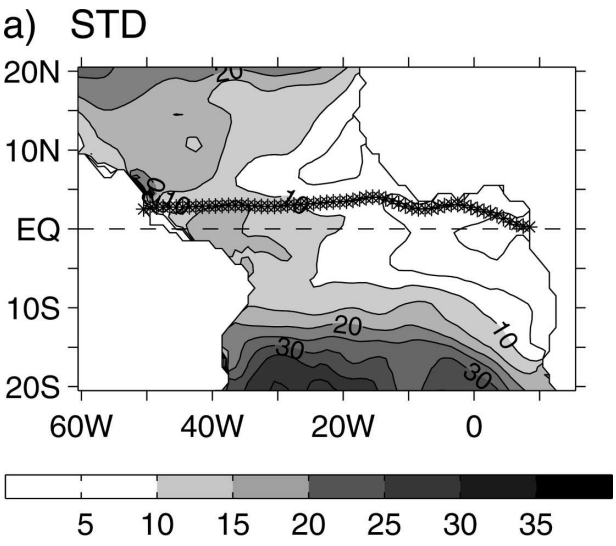


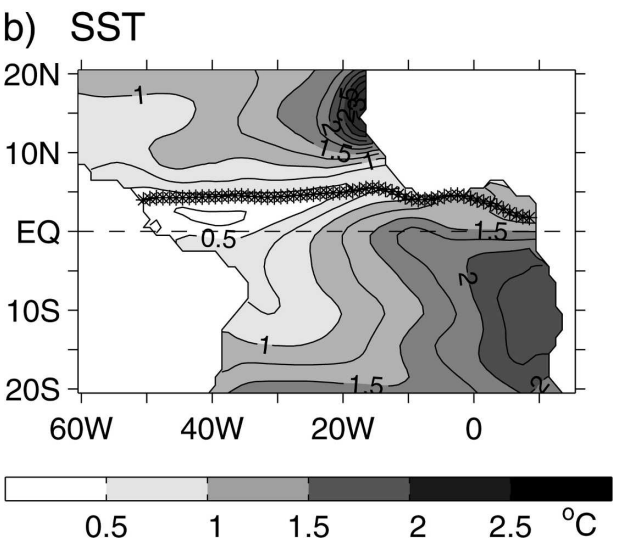


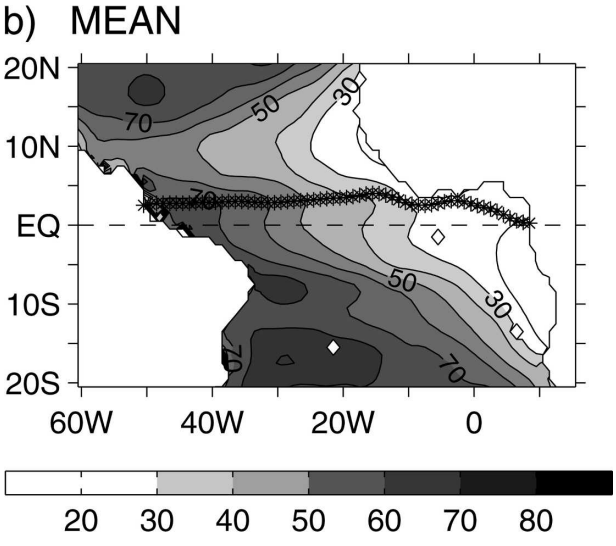


FIG. 4. STD of (a) dSST (contour interval is 0.1°C) and (b) SST (contour interval is 0.25°C). The superimposed thick black line denotes the annual mean position of the ITCZ, which is the average of the monthly mean ITCZ locations. SST data are taken from the OAFlux product.

FIG. 5. (a) STD and (b) annual mean field of $h_{MLD}$ (contour interval is 5m). The data are derived from the WOA temperature analysis. The annual mean position of the ITCZ (thick black line) is superimposed.

superimposed. Annual means are removed from the two variable fields. Interestingly, the area of positive (negative) $Q_{net}$ anomalies matches remarkably well with the area of positive (negative) dSST values throughout the year in the off-equatorial region, with zero $Q_{net}$ contours (marked by bold white lines) in broad agreement with zero dSST contours (marked by bold black lines). It is seen from Figs. 2a and 2b that on the annual mean basis the tropical Atlantic Ocean is a heat gain region in both the OAFux + ISCCP and SOC analyses. Figure 6 shows that the Northern (Southern) Hemispheric part of the basin gains more heat from the atmosphere during March–September (October–March) and receives less heat during the rest of the year. In response, the sea surface tends to warm up (cool down) when $Q_{net}$ is positive (negative).

The relationship between $Q_{net}$ and dSST is, however, less coherent in the equatorial region. Opposite signs between dSST and $Q_{net}$ appear in the extreme eastern equatorial Atlantic in May–June, and extend to a much wider eastern equatorial region in July. The evidence indicates that the atmospheric thermal forcing may not be a direct driver for the cold tongue formation, which is consistent with the theory of Mitchell and Wallace

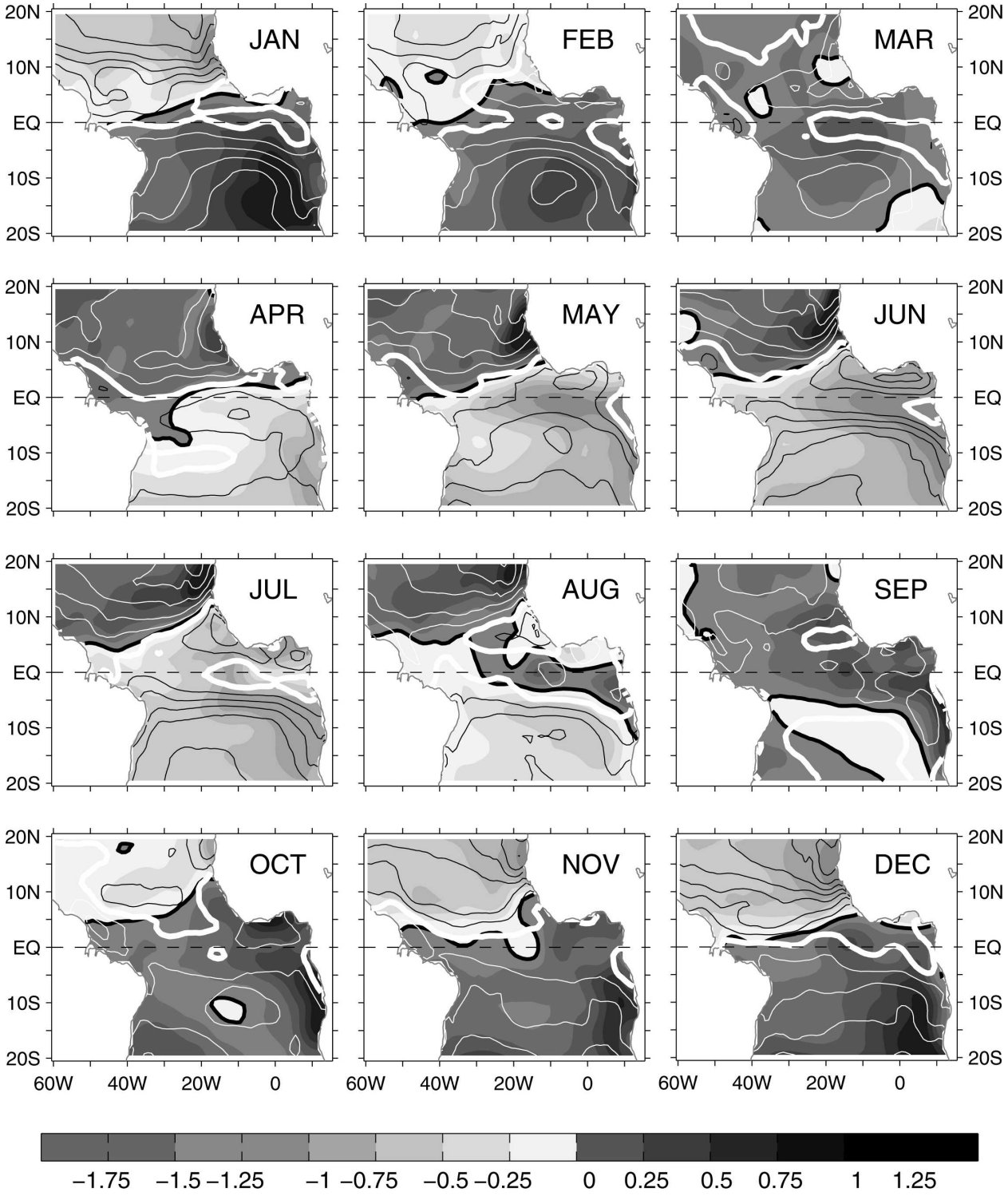


FIG. 6. Monthly evolution of dSST (gray shades; color increment is 0.25°C) with monthly mean $Q_{net}$ superimposed (contours; contour interval is 20 W m$^{-2}$). Both datasets are from the OAFlux product. Positive (negative) dSST is shaded by dark (light) gray colors, while positive (negative) $Q_{net}$ is indicated by white (black) contours. Thick black (white) contours represent zero dSST ($Q_{net}$) values.

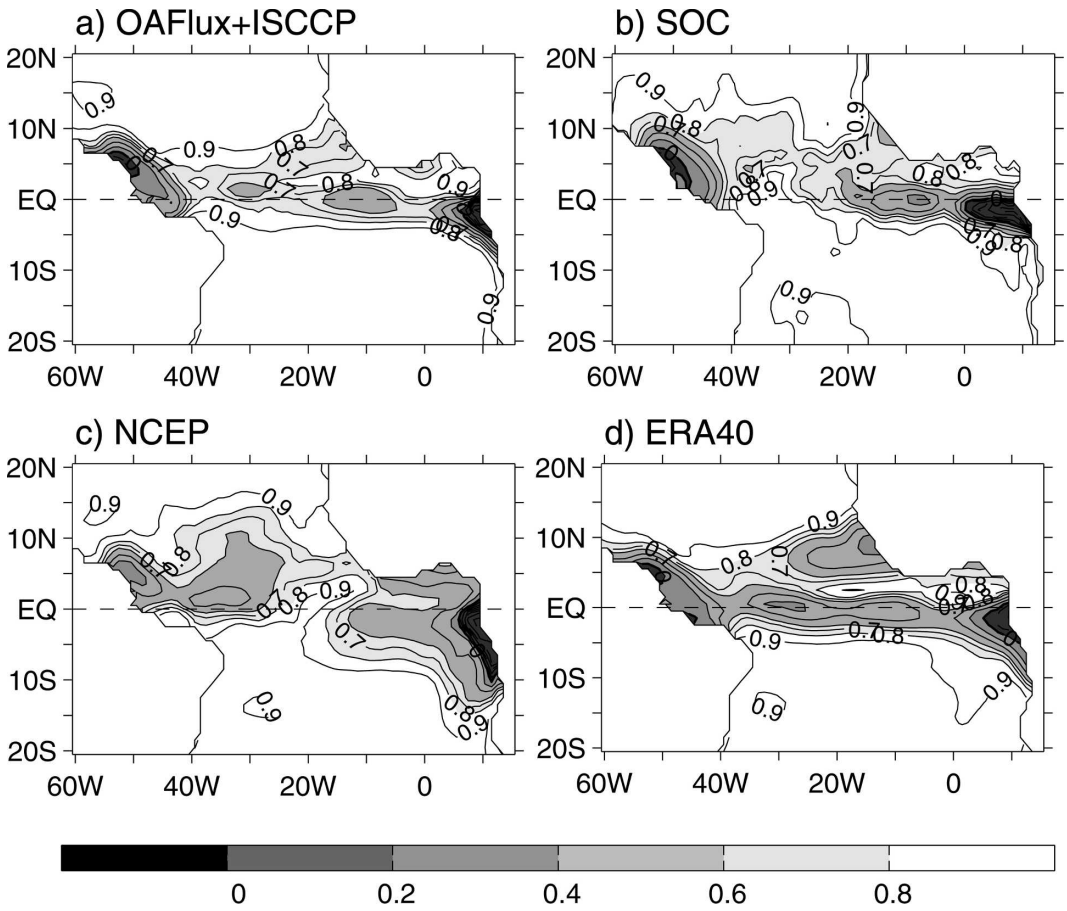


FIG. 7. Correlation <dSST, $Q_{net}$> based on (a) OAFlux + ISCCP, (b) SOC, (c) NCEP–NCAR, and (d) ERA-40. Contour interval is 0.1. The correlation coefficient higher than 0.7 is significant at 99% confidence level.

(1992) that the cold SSTs are produced by upwelling of subsurface water by the onset of the African monsoon.

### *b. Correlation between $Q_{net}$ and dSST*

To compute the statistical significance of the relationship between $Q_{net}$ and dSST (hereafter denoted as $<Q_{net}$ and dSST>) in Fig. 6, the correlation coefficient between the two variable fields is computed (Fig. 7a). Similar plots are also made for the correlation coefficients based on the other three data sources (Figs. 7b–d) so that differences between the four data sources can be evaluated. The correlation $<Q_{net}$ and dSST> from the OAFlux + ISCCP product shows a very interesting feature: the correlation coefficient higher than 0.7 (significant at 99% confidence level) is present everywhere except for the equatorial band between 5°S and 10°N. Within these equatorial latitudes, the relatively low coefficients are grouped into two belts that conjoin in the west with the ring corridor of the North Brazil Current (NBC; Johns et al. 1990; Garzoli et al. 2003) off the northeastern Brazilian coast. One belt of low coefficients is oriented on the equator and spreads southward when reaching the southwestern African coast, and the other is slightly off the equator and tilts to about 10°N near the northwestern African coast. Negative correlation coefficients, denoting that $Q_{net}$ has a phase opposite to that of dSST, occur off the northeastern Brazilian coast and off the southwestern African coast and are embedded in the low correlation belts.

The pattern of the correlation $<Q_{net}$ and dSST> based on the SOC analysis (Fig. 7b) has good agreement with that of OAFlux + ISCCP except for the zonal belt off the equator, where the western part of the belt is broadened and shifted northward. The correlation based on the ERA-40 dataset (Fig. 7c) has the most similar pattern to that of OAFlux + ISCCP, in which the two variables are highly correlated outside of the equatorial region but are weakly or poorly correlated within two zonal belts on and slightly north of the equator. Albeit similar, ERA-40 has much lower correlations in the two zonal belts compared to that of OAFlux + ISCCP. On the other hand, the pattern

based on the NCEP–NCAR dataset is the most different: low correlation coefficients appear over a much wider area. The belt of weak correlation on the equator is intercepted by a sudden bulge of high correlation coefficients (>0.9) near the location at 20°W, and the low coefficient belt north of the equator is widened considerably in the central basin.

The cause of the difference between the four correlation patterns is attributed to $Q_{net}$, not dSST, because of two reasons. The first one is that the STD field of $Q_{net}$ (Fig. 3c) shows that the pattern of the seasonal $Q_{net}$ variance is different between products. In OAFlux + ISCCP and ERA-40, low STD values are confined near the equator; while in SOC and NCEP–NCAR the low STD values cover a wider area; in particular, the STD contour lines in NCEP–NCAR are less zonally aligned both on and off the equator. The second reason is that the SST products from NCEP–NCAR, ERA-40, and OAFlux have essentially the same monthly climatology, because they are all derived from the same source, that is, the weekly mean SST analysis from Reynolds et al. (2002). Although OAFlux analysis includes the direct assimilation of daily AVHRR SST, the monthly SST climatology shows no major difference from the two NWP SST climatologies despite some minor improvement in SST daily variability (Yu et al. 2004a,b). In referring Fig. 7 in the following sections, we exclude the correlation pattern from NCEP–NCAR unless specified.

The cause of the differences between the four sets of $Q_{net}$ is related to the bias of the product. The four products are constructed independently using different methodologies, different datasets, and different bulk flux algorithms (Sun et al. 2003; Yu et al. 2004a,b; Josey 2001). In general, the largest bias source is the COADS data coverage for SOC, model errors for ERA-40 and NCEP–NCAR, the lack of air humidity observations for OAFlux, and the lack of sufficient ground truths for ISCCP. The bias may not have major influence on synoptic weather variability but can significantly impact the estimate of long-term mean and mean seasonal cycle [World Climate Research Program(WCRP)/ Scientific Committee on Ocean Research (SCOR) Working Group on Air–Sea Fluxes (Taylor 2000)]. Clearly, the effort of improving the surface heat flux estimation should be placed more on reducing the mean bias.

## 5. Role of $h_{MLD}$ in modulating the relationship between $Q_{net}$ and dSST

The broad consistency between the three sets of correlation pattern derived from OAFlux + ISCCP, SOC, and ERA-40 (Fig. 7) supports previous studies (Molinari et al. 1985; Houghton 1991; Carton and Zhou 1997; DeWitt and Schneider 1999; Foltz et al. 2003) that $Q_{net}$ is a dominant forcing for seasonal evolution of dSST outside of the equatorial latitudes. As is known, $h_{MLD}$ represents the depth within which the influence of surface heat flux and surface wind stress forcing is concentrated. How does the mixed layer evolve seasonally so that the influence of $Q_{net}$ on dSST can be realized? To examine this issue, we look at the relationship between $h_{MLD}$ and SST on seasonal time scales.

### *a. Role of the mixed layer thermodynamics in the off-equatorial regions*

The correlation between $h_{MLD}$ and SST (hereafter denoted as $<h_{MLD}, SST>$), derived from the WOA monthly climatology, is shown in Fig. 8a. Highly negative correlation coefficients ($<-0.8$) appear in the regions poleward of 10°N and 5°S, and weak, positive correlation coefficients are aligned within the two belt regions: one is located in the central and eastern equatorial basin and the other slightly north of the equator with a northeast tilt toward the northwestern African coast. This correlation pattern is in marked similarity to the pattern of the correlation $<Q_{net}, dSST>$ derived from OAFlux + ISCCP, SOC, and ERA-40 (Fig. 7), but with opposite signs. That is to say that the regions where $h_{MLD}$ and SST are negatively (positively) correlated generally correspond to the regions where $Q_{net}$ and dSST are positively (negatively) correlated. The correspondence is, however, not so clear in the western tropical Atlantic, in the vicinity of the Amazon River mouth.

The two correlation relationships in Figs. 7 and 8a are derived from independent data sources: the $Q_{net}$ and dSST from the flux data centers are produced without the use of $h_{MLD}$ and SST from WOA, and the opposite is also true. Nevertheless, the two correlation patterns are so similar that, when combined, they provide a clear view that in the regions poleward of 10°N and 5°S a warmer (colder) sea surface results from the concentration of larger (smaller) $Q_{net}$ in a thinner (deeper) mixed layer, while the dominance of the $Q_{net}$ forcing in the annual cycle of SST is diminishing when the equator is approached.

The off-equatorial region is the regime where the mixed layer thermodynamics rule: the rise of SST is due to the concentration of large surface heat flux in a shallow mixed layer. This result resonates with previous studies that the sea surface warming is not associated with the increase of the subsurface heat content related to the thermocline deepening (e.g., Merle 1980; Houghton 1991; Reverdin et al. 1997); instead, it is associated

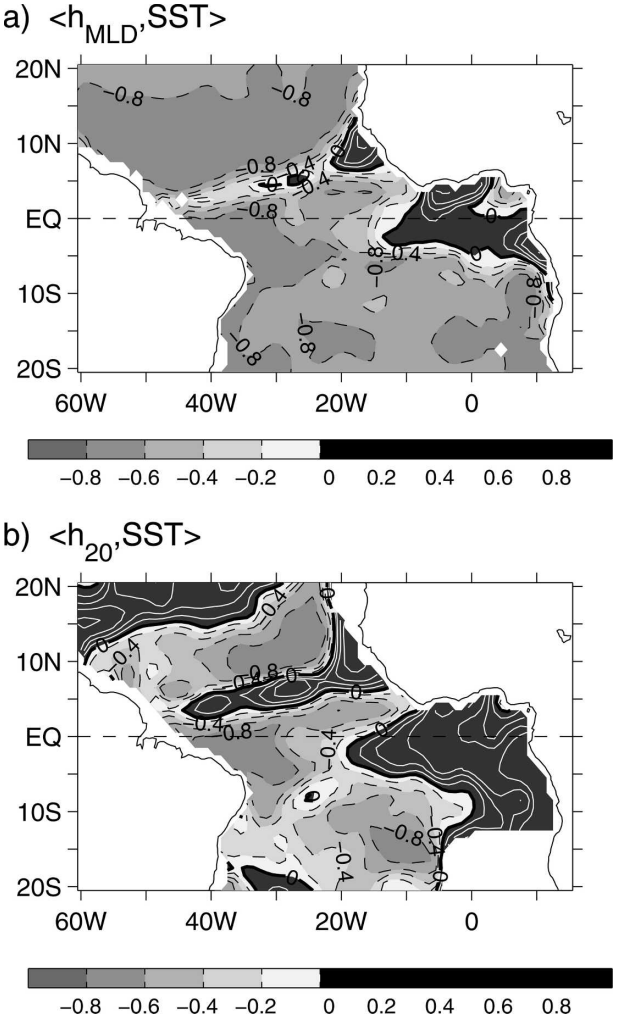


FIG. 8. (a) Correlation $<h_{MLD}$, SST> and (b) correlation $<h_{20}$ and SST>. Contour interval is 0.2. Positive (negative) coefficients are denoted by white solid (black dash) contours. The data are derived from the WOA temperature analysis. The correlation coefficient higher than 0.7 is significant at 99% confidence level.

with the increase of the mixed layer heat content resulting from the increased $Q_{net}$ (Foltz et al. 2003). The governing mechanism for this phenomenon is first proposed by Niiler and Kraus (1977), in which, in the absence of entrainment, the increase of the surface heat flux increases the stability of the mixed layer that generates a stable stratification at the base of the mixed layer and prohibits the mixing with lower water; the mixed layer then becomes effectively decoupled from the thermocline. The importance of surface heat fluxes in controlling seasonal variations of SST via modulating mixing processes in the upper ocean has been demonstrated by the modeling study of the tropical Pacific Ocean (Seager et al. 1988; Giese and Cayan 1993; Köberle and Philander (1994).

### b. *Role of ocean dynamic processes in the equatorial regions*

The influence of $Q_{net}$ on dSST is diminishing as the equator is approached (Fig. 7) and is most evident along the two belts located on and slightly north of the equator. In fact, seasonal variations of SST within the two belts are affected by the changes of the thermocline. To delineate this point, we plot in Fig. 8b the correlation between SST and the depth of the 20°C isotherm (a proxy for the depth of the thermocline), $h_{20}$ (hereafter denoted as $<h_{20}$, SST>). The figure has two features. First, within the equatorial latitudes between 10°S and 10°N, a high, positive correlation $<h_{20}$, SST> occurs in the two exact belt regions where the correlation between $<h_{MLD}$, SST> is weak, suggesting that a warm (cold) SST here is associated with a deep (shallow) thermocline. Second, the correlation $<h_{20}$, SST> is mostly negative in the central basin where the correlation $<h_{MLD}$, SST> is negative, supporting the study of Hastenrath and Merle (1987), wherein a warm SST is related to a shallow mixed layer and a thin and intense thermocline, and our analysis that $Q_{net}$ is a key forcing for seasonal SST variations (Fig. 7).

The high correlation between SST and $h_{20}$ along the off-equator belt within 3°–10°N is linked through the vertical advection associated with the wind-induced Ekman pumping velocity $w_e$ [calculated as $w_e = 1/\rho\ \mathrm{curl}(\tau/f) = 1/(\rho f)\ (\mathrm{curl}(\tau) + \beta\tau^x/f)$]. This occurs because the Ekman velocity affects the time derivative of both $h_{20}$ (a larger upward Ekman pumping velocity tends to lift the thermocline and makes $h_{20}$ shallow) and SST (a larger upward Ekman pumping velocity brings the colder thermocline water to the mixed layer and cools SST). Through this relation, one can expect that $h_{20}$ and the SST are positively correlated. The effect of the Ekman pumping on SST is greatest off the equator in 3°–10°N, due mostly to the fact that the seasonal variance of the wind stress curl is largest (Fig. 9).

The high correlation between SST and $h_{20}$ in the eastern equatorial region is also due to the regulation of the SST by the thermocline movement. The coupled model study (Carton and Zhou 1997; DeWitt and Schneider 1999) suggested that east of 20°W the SST variations along the equator are in direct response to upwelling induced by seasonal enhancement of monsoon wind, while the SST variations from the equator southward off the southwestern Africa coast result from a combination of local wind forcing and remote equatorial wave effects that propagate southward along the coast and affect the thermocline and hence the SST. Because of the important role of oceanic processes in seasonal changes of SST in the deep Tropics between 10°S and

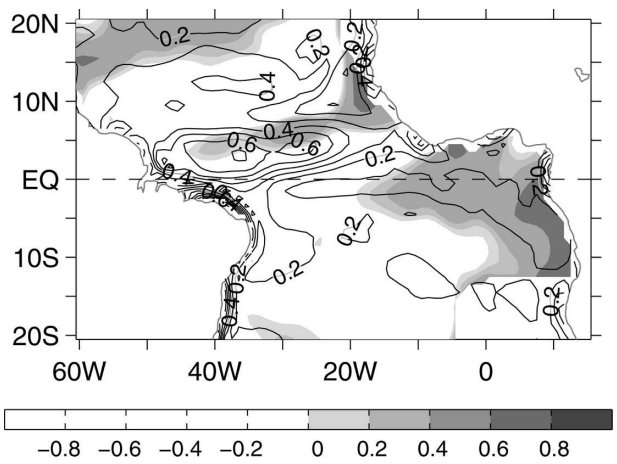


FIG. 9. STD of wind stress curl (black contours; contour interval is $0.2 \times 10^{-7}$ N m$^{-3}$) superimposed onto the correlation $<h_{20}$, SST> (positive coefficients are shaded by gray colors). The wind stress curl is derived from the atlas Special Sensor Microwave Imager (SSM/I) surface wind analysis. The correlation coefficient higher than 0.7 is significant at 99% confidence level.

10°N (Molinari et al. 1985; Weingartner and Weisberg 1991a,b; Foltz et al. 2003), it is not a surprise to see that the correlation between $Q_{\text{net}}$ and dSST is low, particularly within the two belts where the influence of ocean dynamics is most pronounced.

The WOA dataset is known to have bias and the bias can affect the estimation of the mixed layer depth. It should be noted, however, that the characteristics of the seasonal variations of $h_{\text{MLD}}$ in Fig. 8a is a robust feature, and is not affected in any major degree if using a newly developed $h_{\text{MLD}}$ climatology (de Boyer Montegut et al. 2004). The two zonal belt regions of low correlation coefficients are represented in marked similarity by both sets of $h_{\text{MLD}}$ climatology (not shown).

## 6. Predicting seasonal variability of dSST

Given that the annual cycle of dSST in the off-equatorial regions and away from the coast is controlled by the annual cycle of $Q_{\text{net}}$ (Fig. 7), relation (1) can be used to predict dSST by using $Q_{\text{net}}$ and $h_{\text{MLD}}$. In the experiments of this section $Q_{\text{net}}$ is taken from OAFlux + ISCCP and $h_{\text{MLD}}$ from WOA. Figure 10 plots the predicted (black curve) versus the observed (red curve) dSST throughout the course of a year at every 10° in longitude by 3° in latitude grid point over the basin. Differences and similarities between the two curves in the open ocean away from coasts can be summarized as follows:

1) In the regions poleward 10°N and 5°S away from the coast there is a high correlation $<Q_{\text{net}}$, dSST> (Fig. 7). One can see that the model-predicted annual cycle of dSST has phase and amplitude in good agreement with those of the observed dSST. It is safe to say that the response of SST to $Q_{\text{net}}$ is governed by the one-dimensional mixed layer thermodynamic processes (Frankignoul and Hasselmann 1977; Molinari et al. 1985; Houghton 1991; Foltz et al. 2003).
2) Along the equator, the correlation $<Q_{\text{net}}$, dSST> is weak and even becomes negative near the coast of the South Africa. Figure 10 shows that most of the seasonal variability of the observed dSST cannot be produced by the model. The sharp reduction in dSST during the cold tongue establishment in the boreal springtime is clearly not forced by $Q_{\text{net}}$ (Mitchell and Wallace 1992; Carton and Zhou 1997; DeWitt and Schneider 1999; Foltz et al. 2003). Nevertheless, the influence of $Q_{\text{net}}$ on dSST can still be visible to the west of the 20°W in the wintertime, consistent with the observational study of Weingartner and Weisberg (1991a,b) in which the sea surface warming in the boreal winter was in response to a net surface heat flux concentrated by a shallow mixed layer.
3) The region between 3° and 10°N is the only region in the tropical Atlantic that dSST is dominated by a semiannual cycle (Fig. 10), with one maximum in the spring and other in the fall, and a major minimum in the summer and a minor minimum in the winter. The correlation $<Q_{\text{net}}$, dSST> is relatively low (Fig. 7), mostly because $Q_{\text{net}}$ cannot explain the amplitude change of the observed dSST. As shown in Fig. 8b, this is the region that the Ekman pumping effect on SST is large (Yang and Joyce 2006).

## 7. Summary and discussions

The present study uses new surface heat flux products from OAFlux and ISCCP projects to examine two specific issues. First, the study investigated to which degree the surface heat flux governs the seasonal variations of SST in the tropical Atlantic Ocean. Second, the study investigated whether the physical relation [Eq. (1)] can be served as a constraint to characterize the physical representation of heat flux field products. To this regard, the study included the analysis of three additional heat flux products—one is the COADS-based climatology from Southampton Oceanographic Center (SOC; Josey et al. 1998, 1999) and the other two are the NWP model fluxes from National Centers for Environmental Prediction–National Center for Atmospheric Research (NCEP–NCAR; Kalnay et al. 1996)

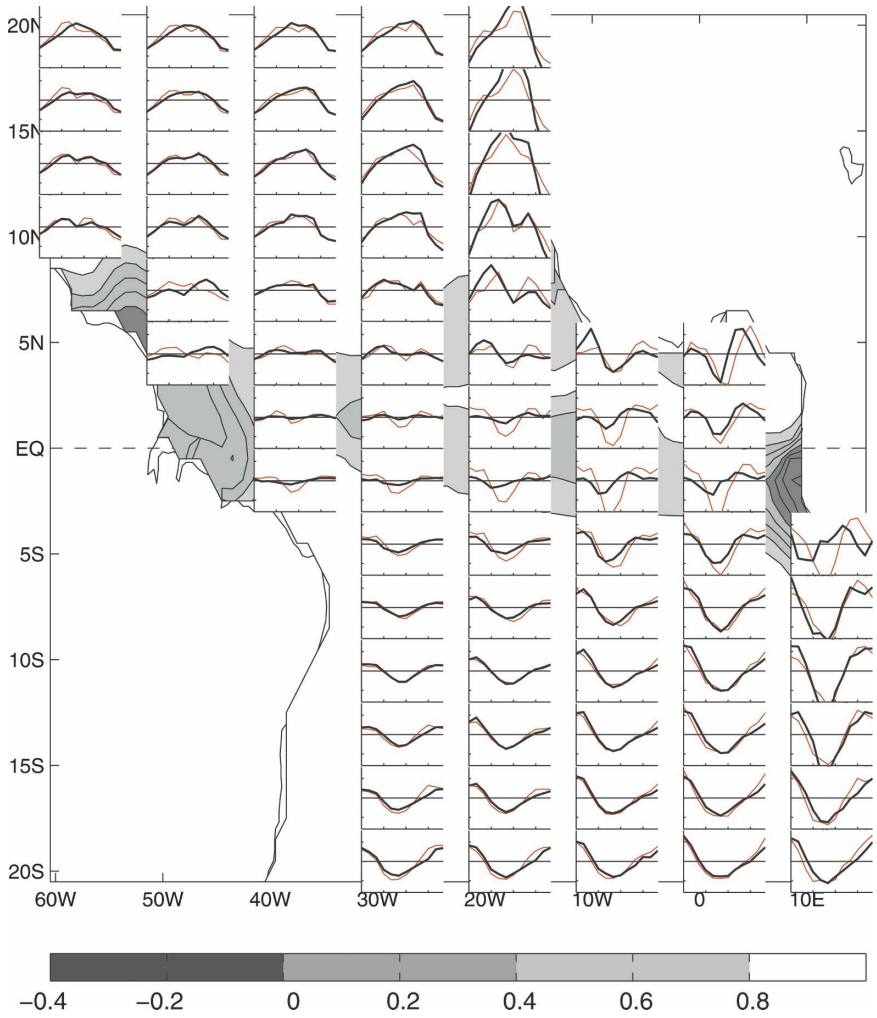


FIG. 10. Model-predicted (black) vs observed (red) dSST. The individual plots are drawn at every 10° in longitude and every 3° in latitude starting from the grid location (60.5°W, 18.5°S). The *x* axis is month and the *y* axis ranges between −1.6° and 1.6°C. The region shaded by gray colors in the background denotes that the correlation $<Q_{net}$, dSST$>$ has a coefficient less than 0.8.

and the 40-yr European Centre for Medium-Range Weather Forecasts (ECMWF) Re-Analysis (ERA-40; Uppala et al. 1999). The study also uses the monthly subsurface temperature fields from WOA to help analyze the seasonal changes of the mixed layer depth.

The comparison of the four $Q_{net}$ products yields the following results:

1) Annual mean (Fig. 2): The annual mean $Q_{net}$ patterns from the four products differ from each other (Sun et al. 2004; Yu et al. 2004b; Josey 2001). Both OAFlux + ISCCP and SOC show that on the annual mean basis the tropical Atlantic sector in the study gains heat from the atmosphere, where the two NWP models, NCEP–NCAR and ERA-40, indicate that positive $Q_{net}$ occurs only along the equatorial belt and in the eastern portion of the tropical basin. Despite the large difference in the mean, all of the products are consistent in that the downward $Q_{net}$ is largest along the equator and $Q_{net}$ decreases toward high north and south latitudes.
2) STD (Fig. 3): Compared to the mean pattern, the four products have a better agreement in producing the pattern and amplitude of seasonal variances of $Q_{net}$. All of the products show that the amplitude of the $Q_{net}$ seasonal variations is smallest along the equatorial band between 5°S and 5°N and off the southwestern African coasts, and the amplitude in-

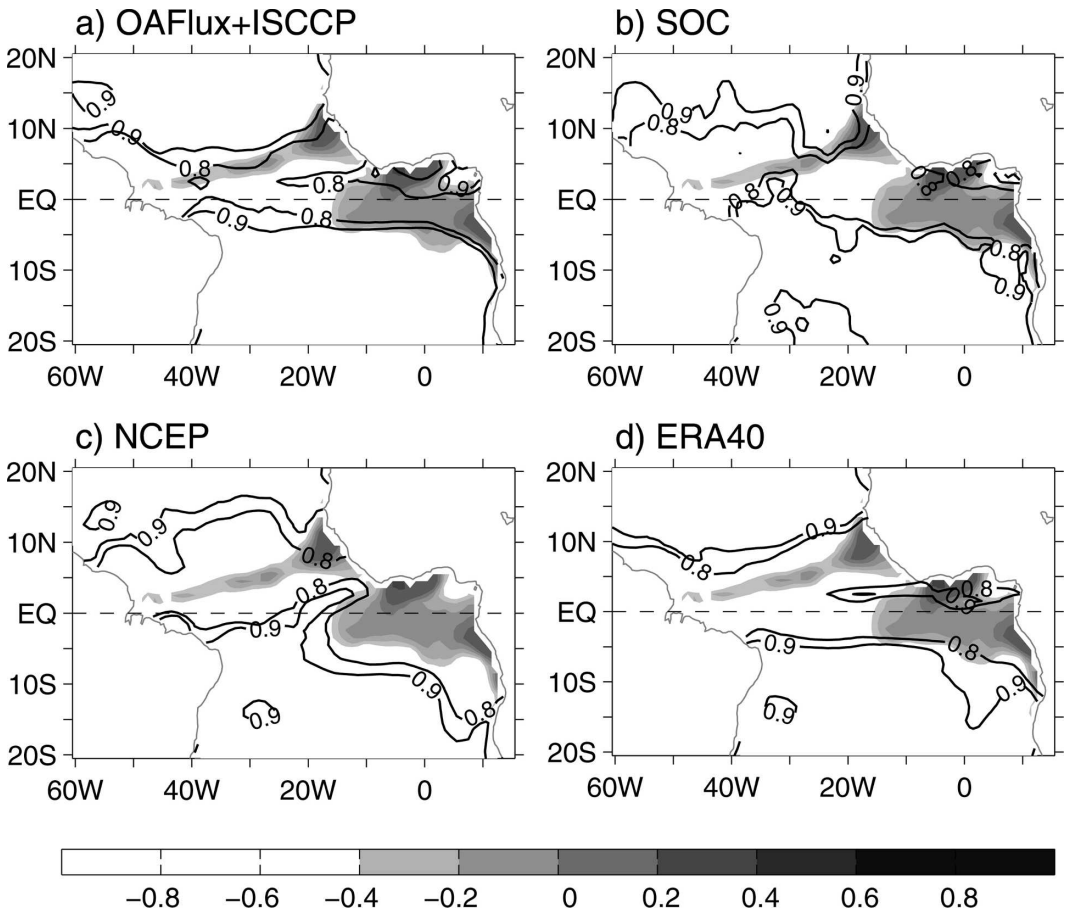


FIG. 11. Superimposition of the correlation $<h_{MLD}$, SST> (coefficients greater than −0.5 are shaded by gray colors) onto the location of the correlation $<Q_{net}$, dSST> with coefficient at 0.9 (black contour). The correlation $<Q_{net}$, dSST> with coeffiencts of 0.8 and 0.9 is plotted for (a) OAFlux + ISCCP, (b) SOC, (c) NCEP–NCAR, and (d) ERA-40.

creases poleward away from the equator. Despite the broad similarity, NCEP–NCAR differs from the other three products in that the STD distribution is less zonally oriented in the central basin.

3) Role of $Q_{net}$ in seasonal variability of dSST (Fig. 7): The correlation $<Q_{net}$, dSST> based on the three products, OAFlux + ISCCP, SOC, and ERA-40, produce a similar pattern, in which high correlation coefficients appear in the region outside of the deep Tropics (in the case, 5°S – 10°N) and low coefficients are located along two belt regions, with one on the equator and the other slightly off the equator from 3°N at 40°W to about 10°N near the northwestern African coast. The two low coefficient belts conjoin in the west with the ring corridor of the NBC (Johns et al. 1990; Garzoli et al. 2003) off the northeastern Brazilian coast. The correlation based on NCEP–NCAR $Q_{net}$ and dSST shows low coefficients in a much wider area, considerably different from the other three products. The cause of the difference is attributed to the pattern of NCEP–NCAR $Q_{net}$ (Fig. 3).

4) Summary: When the four patterns of the correlation $<Q_{net}$, dSST> are superimposed onto the independent set of the correlation $<h_{MLD}$, SST> derived from the subsurface WOA database (Levitus and Boyer 1994) (Fig. 11), one can see that low (high) $<Q_{net}$, dSST> coefficients from the two flux products, OAFlux + ISCCP and ERA-40, occur in the exact region where the correlation $<h_{MLD}$, SST> is weakly (highly) negative. If the degree of consistency between the correlation $<Q_{net}$, dSST> and the correlation $<h_{MLD}$, SST> is a measure of the physical representation of the $Q_{net}$ product, then, apparently, the seasonal variations of $Q_{net}$ are best produced by OAFlux + ISCCP and ERA-40, followed by SOC. The NCEP–NCAR $Q_{net}$ is least representative.

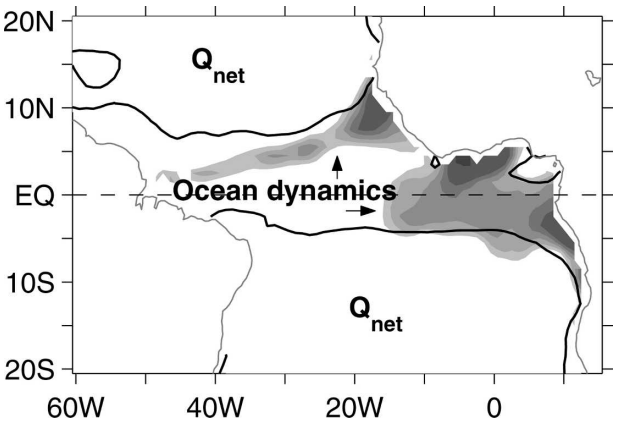


FIG. 12. Schematic diagram of the dominant influence of $Q_{net}$ and ocean dynamic processes in seasonal variations of SST based on the 0.9 correlation coefficient of $<Q_{net}$, dSST$>$ derived from the OAFlux product. The role of oceanic process is deemed important in the two zonal belts (gray color shaded) of the equatorial Atlantic Ocean.

Regarding the role of $Q_{net}$ in the seasonal evolution of SST, we found that the tropical Atlantic sector can be divided into two regimes based on the correlation $<Q_{net}$, dSST$>$ at 0.9 derived from OAFlux + ISCCP and ERA-40. A schematic diagram is drawn in Fig. 12 and the description is given as follows:

1) The annual cycle of dSST in the regions poleward of 10°N and 5°S is dominated by the annual cycle of $Q_{net}$, consistent with previous observational and modeling studies (Molinari et al. 1985; Houghton 1991; Carton and Zhou 1997; DeWitt and Schneider 1999; Foltz et al. 2003). In these regions the warming (cooling) of the sea surface results from the concentration of the increased (decreased) net surface heat flux in a relatively shallow (deep) mixed layer (Figs. 7 and 8). The seasonal evolution of dSST can be well predicted by Eq. (1) using OAFlux + ISCCP $Q_{net}$ (Fig. 10).
2) The deep Tropics between 5°S and 10°N is the regime where the seasonal changes of SST are governed by ocean dynamic processes. The dynamics-induced changes in SST are most evident along the two belts—one of which is located on the equator (Weingartner and Weisberg 1991a,b) and the other is off the equator at about 3°N in the west and tilts to about 10°N near the northwestern African coast (Garzoli and Katz 1983; Molinari et al. 1985; Yang and Joyce 2006). Within the two belt regions, the seasonal variations of SST are in response to the changes of the thermocline induced by surface wind forcing.
3) Summary: The analysis is consistent with previous observational studies of Molinari et al. (1985) and Houghton (1991) wherein in most of the tropical Atlantic Ocean the major contributor to the surface mixed layer heat budget is not the vertical flux of heat through the thermocline, but the net surface heat flux through the air–sea interface. This indicates that a shallow thermocline does not necessarily facilitate the cooling of the mixed layer; instead, it can foster a warming of the sea surface. The analysis is also in good agreement with existing literature that the annual cycle of the SST along the equator is controlled not by surface heat flux but the oceanic response to monsoonal forcing (Weingartner and Weisberg 1991a,b; Mitchell and Wallace 1992; Carton and Zhou 1997; DeWitt and Schneider 1999). The analysis has clearly identified that the tilted belt from 3°N in the west to 10°N near the northwestern African coast is the other region where the changes in SST are controlled by ocean dynamics (Garzoli and Katz 1983; Molinari et al. 1985; Yang and Joyce 2006).

In summary, the study demonstrates that $Q_{net}$ formed from the newly developed OAFlux and ISCCP products gives a more realistic quantification of the correlation between dSST and $Q_{net}$. By comparison, other flux products are less good. The study suggests that an accurate estimation of surface heat flux is crucially important. It can enhance the understanding of the mechanisms controlling seasonal SST variations in the tropical Atlantic Oceans; it can enhance and extend previous studies that are based on models and/or limited in situ observations; and it can help to develop seasonal prediction skills for SST. The study also suggests that future emphasis on improving the surface heat flux estimation should be placed more on reducing the mean bias.

*Acknowledgments.* This study is support by the NOAA CLIVAR Atlantic under Grant NA06GP0453 and NOAA Climate observations and Climate Change and Data Detection under Grant NA17RJ1223. Bill Rossow is acknowledged for providing ISCCP-FD dataset and Simon Josey for the SOC climatology. *World Ocean Atlas 1994* data and NCEP–NCAR reanalysis are provided by the NOAA–CIRES Climate Diagnostics Center, Boulder, Colorado, from their Web site (available online at http://www.cdc.noaa.gov). ERA-40 is obtained from the Data Support Section at National Center of Atmospheric Research (NCAR).

## REFERENCES

Chang, P., 1996: The role of the dynamic ocean–atmosphere interactions in the tropical seasonal cycle. *J. Climate,* **9,** 2973–2998.

——, and G. Philander, 1994: A coupled ocean–atmosphere instability of relevance to the seasonal cycle. *J. Atmos. Sci.,* **51,** 3628–3648.

Carton, J. A., and Z. X. Zhou, 1997: Annual cycle of sea surface temperature in the tropical Atlantic Ocean. *J. Geophys. Res.,* **102,** 27 813–27 824.

de Boyer Montegut, C., G. Madec, A. S. Fischer, A. Lazar, and D. Iudicone, 2004: Mixed layer depth over the global ocean: An examination of profile data and a profile-based climatology. *J. Geophys. Res.,* **109,** C12003, doi:10.1029/2004JC002378.

DeWitt, D. G., and E. K. Schneider, 1999: The processes determining the annual cycle of equatorial sea surface temperature: A coupled general circulation model perspective. *Mon. Wea. Rev.,* **127,** 381–395.

Foltz, G. R., S. A. Grodsky, J. A. Carton, and M. J. McPhaden, 2003: Seasonal mixed layer heat budget of the tropical Atlantic Ocean. *J. Geophys. Res.,* **108,** 3146, doi:10.1029/2002JC001584.

Frankignoul, C., and K. Hasselmann, 1977: Stochastic climate models, 2: Application to sea-surface temperature anomalies and thermocline variability. *Tellus,* **29,** 289–305.

Garzoli, S. L., and E. J. Katz, 1983: The forced annual reversal of the Atlantic north equatorial countercurrent. *J. Phys. Oceanogr.,* **13,** 2082–2090.

——, A. Ffield, and Q. Yao, 2003: North Brazil Current rings and the variability in the latitude of the retroflection. *Interhemispheric Water Exchanges in the Atlantic Ocean,* J. Goni and P. Malanotte-Rizzoli, Eds., Elsevier Oceanographic Series, Vol. 68, Elsevier, 357–373.

Giese, B. S., and D. R. Cayan, 1993: Surface heat flux parameterizations and tropical Pacific sea surface temperature simulations. *J. Geophys. Res.,* **98,** 6979–6989.

Hastenrath, S., 1984: Interannual variability and the annual cycle: Mechanisms of circulation and climate in the tropical Atlantic sector. *Mon. Wea. Rev.,* **112,** 1097–1107.

——, and P. J. Lamb, 1978: *Heat Budget Atlas of the Tropical Atlantic and Eastern Pacific Oceans.* University of Wisconsin Press, 103 pp.

——, and J. Merle, 1987: Annual cycle of subsurface thermal structure in the Tropical Atlantic Ocean. *J. Phys. Oceanogr.,* **17,** 1518–1538.

Houghton, R. W., 1983: Seasonal-variations of the subsurface thermal structure in the Gulf of Guinea. *J. Phys. Oceanogr.,* **13,** 2070–2081.

——, 1991: The relationship of sea surface temperature to thermocline depth at annual and interannual time series in the tropical Atlantic Ocean. *J. Geophys. Res.,* **96** (C8), 15 173–15 185.

Johns, W. E., T. N. Lee, F. A. Schott, R. J. Zantopp, and R. H. Evans, 1990: The North Brazil Current retroflection seasonal structure and eddy variability. *J. Geophys. Res.,* **95,** 22 103–22 120.

Josey, S. A., 2001: A comparison of ECMWF and NCEP/NCAR surface heat fluxes with moored buoy measurements in the subduction region of the North-East Atlantic. *J. Climate,* **14,** 1780–1789.

——, E. C. Kent, and P. K. Taylor, 1998: *The Southampton Oceanography Centre (SOC) Ocean-Atmosphere Heat, Momentum and Freshwater Flux Atlas*. Rep. 6, Southampton Oceanography Centre, 30 pp. + figs.

——, ——, and ——, 1999: New insights into the ocean heat budget closure problem from analysis of the SOC air-sea flux climatology. *J. Climate,* **12,** 2685–2718.

Joyce, T. M., C. Frankignoul, J. Yang, and H. E. Phillips, 2004: Ocean response and feedback to the SST dipole in the tropical Atlantic. *J. Phys. Oceanogr.,* **34,** 2525–2540.

Kalnay, E., and Coauthors, 1996: The NCEP/NCAR 40-Year Reanalysis Project. *Bull. Amer. Meteor. Soc.,* **77,** 437–471.

Katz, E. J., 1987: Seasonal response of the sea surface to the wind in the equatorial Atlantic. *J. Geophys. Res.,* **92,** 1885–1893.

Köberle, C., and S. G. H. Philander, 1994: On the processes that control seasonal variations of sea surface temperatures in the tropical Pacific Ocean. *Tellus,* **46A,** 481–496.

Leetmaa, A., 1983: The role of local heating in producing temperature variations in the offshore waters of the eastern tropical Pacific. *J. Phys. Oceanogr.,* **13,** 467–473.

Levitus, S., and T. P. Boyer, 1994: *Temperature*. Vol. 4, *World Ocean Atlas 1994,* NOAA Atlas NESDIS 4, 117 pp.

McPhaden, M. J., 1982: Variability in the Central equatorial Indian Ocean-Part I: Ocean dynamics. *J. Mar. Res.,* **40,** 157–176.

Merle, J., 1980: Seasonal heat budget in the equatorial Atlantic Ocean. *J. Phys. Oceanogr.,* **10,** 464–469.

——, and S. Arnault, 1985: Seasonal variability of the surface dynamic topography in the tropical Atlantic Ocean. *J. Mar. Res.,* **43,** 267–288.

Mitchell, T. P., and J. M. Wallace, 1992: On the annual cycle in equatorial convection and sea surface temperature. *J. Climate,* **5,** 1140–1156.

Moisan, J., and P. Niiler, 1998: The seasonal heat budget of the North Pacific: Net heat flux and heat storage rates (1950–90). *J. Phys. Oceanogr.,* **28,** 401–421.

Molinari, R. L., J. F. Festa, and E. Marmolejo, 1985: Evolution of sea surface temperature in the tropical Atlantic Ocean during FGGE, 1979, II. Oceanographic fields and heat balance of the mixed layer. *J. Mar. Res.,* **43,** 67–81.

Nigam, S., and Y. Chao, 1996: Evolution dynamics of tropical ocean–atmosphere annual cycle variability. *J. Climate,* **9,** 3187–3205.

Niiler, P. P., and E. B. Kraus, 1977: One-dimensional models of the upper ocean. *Modelling and Prediction of the Upper Layers of the Ocean,* E. B. Kraus, Ed., Pergamon, 143–172.

Philander, G., D. Gu, D. Halpern, G. Lambert, N.-C. Lau, T. Li, and R. C. Pacanowski, 1996: Why the ITCZ is mostly north of the equator. *J. Climate,* **9,** 2958–2972.

Reverdin, G., D. Cayan, and Y. Kushnir, 1997: Decadal variability of hydrography in the upper northern North Atlantic, 1948–1990. *J. Geophys. Res.,* **102,** 8505–8532.

Reynolds, R. W., N. A. Rayner, T. M. Smith, D. C. Stokes, and W. Wang, 2002: An improved in situ and satellite SST analysis for climate. *J. Climate,* **15,** 1609–1625.

Richardson, P. L., and G. Reverdin, 1987: Seasonal cycle of velocity in the Atlantic North Equatorial Countercurrent as measured by surface drifters, current meters, and ship drifts. *J. Geophys. Res.,* **92,** 3691–3708.

Seager, R., S. E. Zebiak, and M. A. Cane, 1988: A model of the tropical Pacific sea surface temperature climatology. *J. Geophys. Res.,* **93,** 1265–1280.

Sun, B., L. Yu, and R. A. Weller, 2003: Comparisons of surface meteorology and turbulent heat fluxes over the Atlantic: NWP model analyses versus moored buoy observations. *J. Climate,* **14,** 679–695.

Taylor, P. K., Ed., 2000: Intercomparison and validation of ocean-atmosphere energy flux fields—Final report of the Joint WCRP/SCOR Working Group on Air-Sea Fluxes. WGASF, WCRP-112, WMO/TD-1036, 306 pp.

Uppala, S., J. K. Gibson, M. Fiorino, A. Hernandez, P. Kallberg,

L. Xu, K. Onogi, and S. Saarinen, 1999: ECMWF second generation re-analysis ERA40. *Proc. of the Second WCRP Int. Conf. on Re-Analyses,* Wokefield Park, Reading, United Kingdom, WCRP, 9–13.

Wang, B., 1994: On the annual cycle in the tropical eastern central Pacific. *J. Climate,* **7,** 1926–1942.

Wang, C., and D. B. Enfield, 2001: The tropical Western Hemisphere warm pool. *Geophys. Res. Lett.,* **28,** 1635–1638.

Weingartner, T. J., and R. H. Weisberg, 1991a: On the annual cycle of equatorial upwelling in the central Atlantic Ocean. *J. Phys. Oceanogr.,* **21,** 68–82.

——, and ——, 1991b: A description of the annual cycle in sea surface temperature and upper ocean heat in the equatorial Atlantic. *J. Phys. Oceanogr.,* **21,** 83–96.

Woodruff, S. D., S. J. Lubker, K. Wolter, S. J. Worley, and J. D. Elms, 1993: Comprehensive Ocean-Atmosphere Data Set (COADS) Release 1a: 1980-92. *Earth Syst. Monitor,* **4,** 1–8.

Xie, P., and P. A. Arkin, 1997: Global precipitation: A 17-year monthly analysis based on gauge observations, satellite estimates and numerical model outputs. *Bull. Amer. Meteor. Soc.,* **78,** 2539–2558.

Xie, S.-P., 1994: On the genesis of the equatorial annual cycle. *J. Climate,* **7,** 2008–2013.

——, and J. A. Carton, 2004: Tropical Atlantic variability: Patterns, mechanisms, and impacts. *Earth Climate: The Ocean-Atmosphere Interaction, Geophys. Monogr.,* Vol. 147, Amer. Geophys. Union, 121–142.

Yang, J., and T. M. Joyce, 2006: Local and equatorial forcing of seasonal variations of the North Equatorial Countercurrent in the Atlantic Ocean. *J. Phys. Oceanogr.,* **36,** 238–254.

Yu, L., R. A. Weller, and B. Sun, 2004a: Improving latent and sensible heat flux estimates for the Atlantic Ocean (1988-1999) by a synthesis approach. *J. Climate,* **17,** 373–393.

——, ——, and ——, 2004b: Mean and variability of the WHOI daily latent and sensible heat fluxes at in situ flux measurement sites in the Atlantic Ocean. *J. Climate,* **17,** 2096–2118.

Zhang, Y.-C., W. B. Rossow, A. A. Lacis, V. Oinas, and M. I. Mishchenko, 2004: Calculation of radiative fluxes from the surface to top of atmosphere based on ISCCP and other global data sets: Refinements of the radiative transfer model and the input data. *J. Geophys. Res.,* **109,** D19105, doi:10.1029/2003JD004457.